TU Delft

Delft University of Technology

The making of the dirk

What can chemical analysis and imaging techniques tell us

Joosten, Ineke; Megens, Luc; Beentjes, Tonny; Amkreutz, Luc; Li, Y.; van Eijck, L.

Publication date
2024

Document Version
Final published version

Published in
Larger than Life

Citation (APA)
Joosten, I., Megens, L., Beentjes, T., Amkreutz, L., Li, Y., & van Eijck, L. (2024). The making of the dirk: What can chemical analysis and imaging techniques tell us. In L. W. S. W. Amkreut, & D. Fontijn (Eds.), *Larger than Life: The Ommerschans hoard and the role of giant swords in the European Bronze Age (1500-1100 BC)* (pp. 107-118). Sidestone Press.

Important note
To cite this publication, please use the final published version (if applicable).
Please check the document version above.

Copyright
Other than for strictly personal use, it is not permitted to download, forward or distribute the text or part of it, without the consent of the author(s) and/or copyright holder(s), unless the work is under an open content license such as Creative Commons.

Takedown policy
Please contact us and provide details if you believe this document breaches copyrights.
We will remove access to the work immediately and investigate your claim.

This work is downloaded from Delft University of Technology.
For technical reasons the number of authors shown on this cover page is limited to a maximum of 10.

Chapter 6

The making of the dirk: What can chemical analysis and imaging techniques tell us

Ineke Joosten, Luc Megens, Tonny Beentjes, Luc Amkreutz, Yueer Li and Lambert van Eijck

6.1 Introduction

The dirk of Ommerschans seems to be of an exceptional quality. Its size and the smooth surface suggest that it was a one of kind object. However, five similar shaped dirks of this period have been found, suggesting that these were made in series (e.g. Fontijn 2001; this volume). The beautifully coloured surface of the Ommerschans specimen we appreciate so much today, is the result of being buried in bog peat for over 3000 years and, after excavation, being on show for over one hundred years without climate control. The latter might not have been of major influence since the current surface is very comparable to that of a replica of the dirk made in 1927, about 30 years after its discovery (Chapter 2).[1] The exceptional nature of this dirk and the five other similar dirks found on the European continent and in Great Britain and the assumption that they were made for ceremonial purposes, led us to further investigate the production process and potential use of the Ommerschans dirk by means of analytical and imaging techniques. The research questions considered are listed in the following.

6.1.1 What can be said about the mould and the material that this mould was made of?

During the Bronze Age several types of moulds, made of different materials, were in use (Kuijpers 2008). Objects could be cast in open and closed moulds, bi-valve moulds, piece moulds and using the lost wax method. With possible mould materials such as bronze, natural stone, loam and perhaps sand. The latter method is not confirmed by any archaeological evidence from this period, most likely because it does not leave any traces. Also, suitable moulding/casting sand is only found in a few places worldwide (Beentjes 2019). In addition, this method also requires a frame to hold the sand.

1 A plaster cast of the sword was made which was subsequently painted to mimic the surface colours of the sword. Plaster casts in those days were made with gelatine or plaster. No remains are visible in the pores of the dirk now.

in: Amkreutz, L.W.S.W. and Fontijn, D.R. (eds) 2024. *Larger than Life. The Ommerschans hoard and the role of giant swords in the European Bronze Age (1500-1100 BC).* Leiden: Sidestone Press (= *Papers on Archaeology of the Leiden Museum of Antiquities Leiden* 30), pp. 107-118.

Remains of such frames are not found before 1400 AD and textual and pictorial sources from antiquity and the Middle Ages do not provide evidence for casting in sand, only in loam (Beentjes 2019). In the Netherlands, moulds made of clay, loam and bronze have been found dating from the Bronze Age (Kuijpers 2008). Loam seems to be a very suitable method to cast objects with an ornamental surface (Beentjes 2019). For instance, bells were cast well into the 20th century using loam moulds (Jennings 1988). Most likely a wooden model was made first. Wood is readily available, easily worked into a thin and smooth model, but unfortunately its use leaves no traces behind. In the Bronze Age metal moulds appear to have been used mainly for the production of axes (Baron *et al.* 2014). Only a few examples of stone moulds (i.e. sandstone and soapstone) are known to have been used in Europe (Pola *et al.* 2015).

6.1.2 How was the dirk cast?

Several computer simulations exist of the casting of archaeological bronze objects dating from the Bronze Age to the Roman period (Garbacz-Klempka *et al.* 2017; Kowalski *et al.* 2019; Pola *et al.* 2015; Willer *et al.* 2016/2017). These simulations are based on careful CT scans of objects or moulds and take the chemical composition of the alloy and the mould material into account. The results suggest that the position of the defects in the metal reveal information on how an object was cast in terms of temperature of the metal, the direction of the pour, the position of the gating system and the mould material. During casting of a bronze object, two types of cavities can form: air bubbles which have a round shape and pores which are the result of the shrinkage of the cooling metal and typically have an irregular outline. Air bubbles can originate from the pouring action of the metal in the mould or due to the evaporation of moisture or gasses from burned organic material from the mould material when this was not properly preheated (Garbacz-Klempka *et al.* 2017; Kuijpers 2008; Pola *et al.* 2015). In general, shrinkage defects will occur at places where the metal is thicker and takes longer to solidify or at places where there are large differences in thickness or volume resulting in stress cracks in the cast (Pola *et al.* 2015).

6.1.3 Was the surface of the dirk worked afterwards?

Post-casting treatments may have been applied. The surface can be worked by cold hammering to harden the metal (Sáez and Lerma 2015). Finishing processes like whetting to sharpen the edge(s) of the dirk and polishing to give the surface smoothness and enhance its metallic lustre. Tool marks usually appear as regular, straight or curved grooves on the metal surface.

6.1.4 Are there any signs of use or wear?

Tool marks, rounding, edge deformation and the formation of notches are typical of wear through use (Sáez and Lerma 2015). When looking for these signs, corrosion and conservation treatments must also be taken into account since these can obscure or even obliterate signs of use-wear. To investigate these issues, the dirk was studied non-invasively using 3D microscopy (OM) and X-ray fluorescence (XRF). X-radiography and neutron tomography (nCT) was employed to study inner defects that are invisible from the outside.

6.2 Experimental methods

Digital 3D microscopy was used to study the surface of the dirk. The instruments used are a Hirox KH-7700 Digital Microscope, with visible light as source, and a Foster & Freeman Video Spectral Comparator (VSC) 8000, which combines multiple wavelengths (UV/visual/IR).

X-ray radiography was used to reveal defects in the body of the dirk providing two-dimensional images. To ensure a stable positioning of the dirk during the X-ray imaging, it was positioned in its wooden transport box. The overall length of the object is 68 centimetres, therefore it is larger than the field of view of the used set-up. The X-ray images were carried out in six height steps to ensure that the entire object was covered within the recorded images and to provide comfortable overlaps between the different images. The broadened part of the blade, where a hilt would have been attached if the dirk would have been used as a weapon, was recorded in three steps since the width of 18 centimetres is also larger than the field of view. The instrument used is a General Electric Eresco 280 MF, with a rotating table, 2 millimetres thick copper filter and BIX- and FP-detectors. Images were made at 150 and 180 kilovolt.

Neutron tomography (nCT) was performed to non-invasively access the interior structure of the dirk. The principle of nCT is very similar to X-ray CT-scans as used for medical purposes, with the main difference being the capability of neutron radiation to penetrate thick metal objects. This experiment was performed at the research reactor of TU Delft (Zhou *et al.* 2018). Because the dirk is considerably bigger than the FISH neutron beam cross-section, the experiment was repeat at five different positions along the length of the dirk. After standard computer-reconstruction of the data, these five 3D models are then stitched into one 3D model. The instrumental spatial resolution for this experiment was approximately 0.4 millimetres.

A Bruker M6 JETSTREAM (macro-set-up) was used for mapping the chemical composition of the entire surface of the dirk. The system is equipped with a Rh-target microfocus X-ray tube that was set at the maximum

Figure 6.1: Examination spots on the dirk with the Hirox microscope (T. Han).

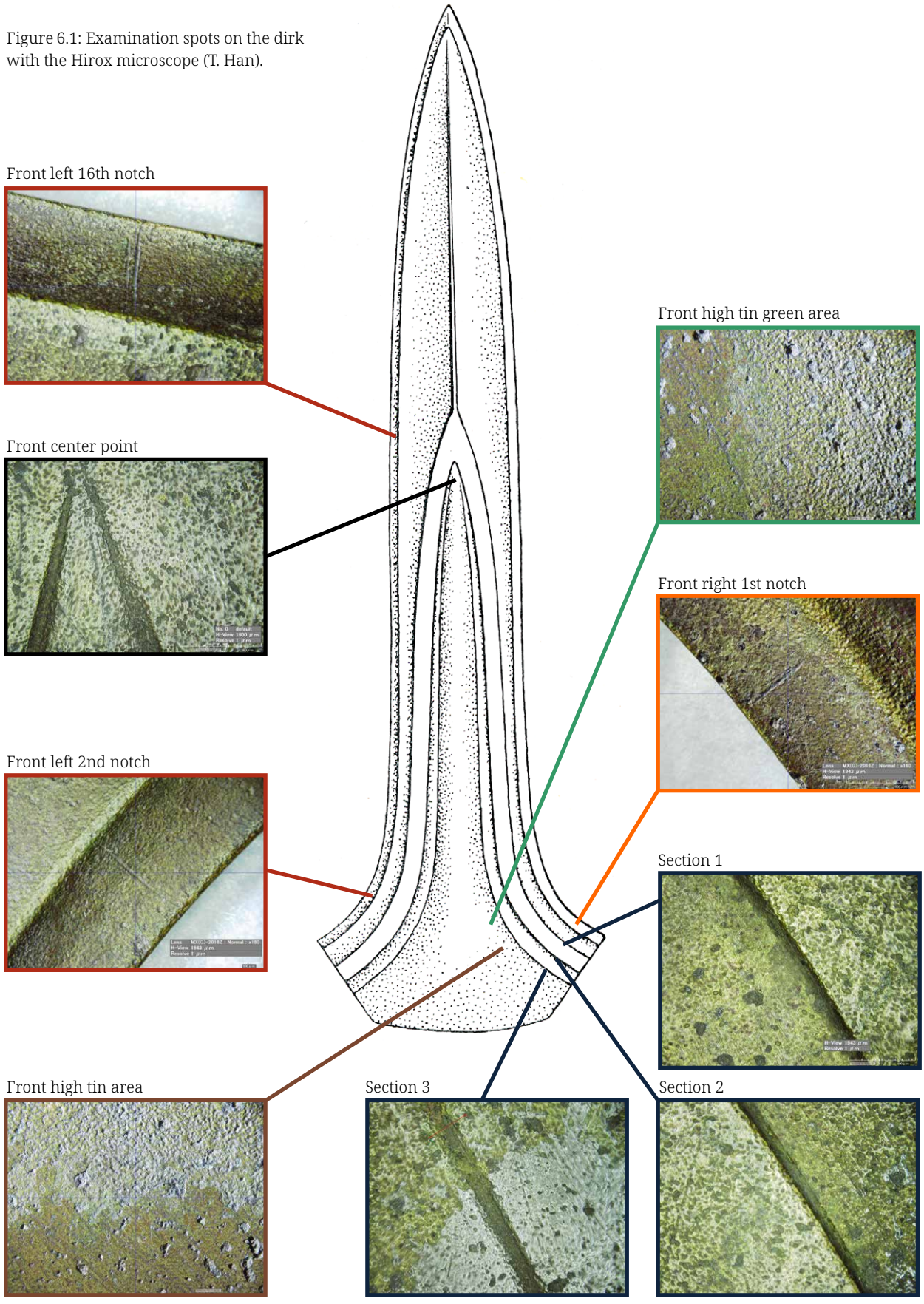

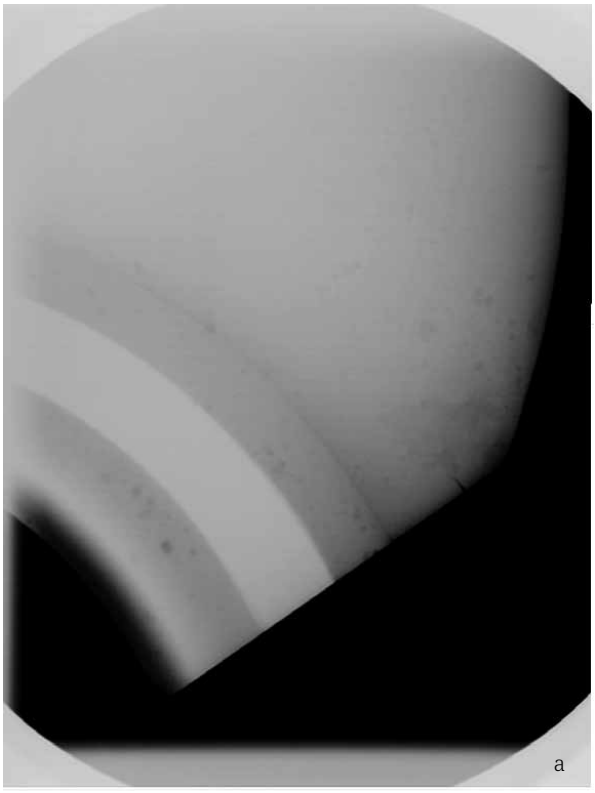

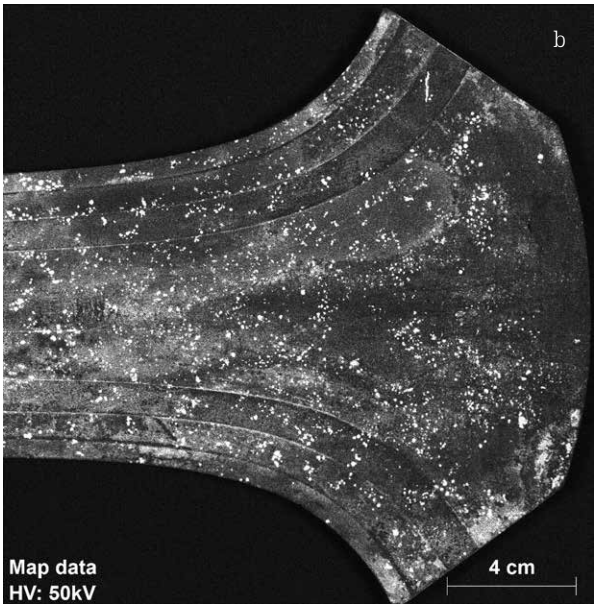

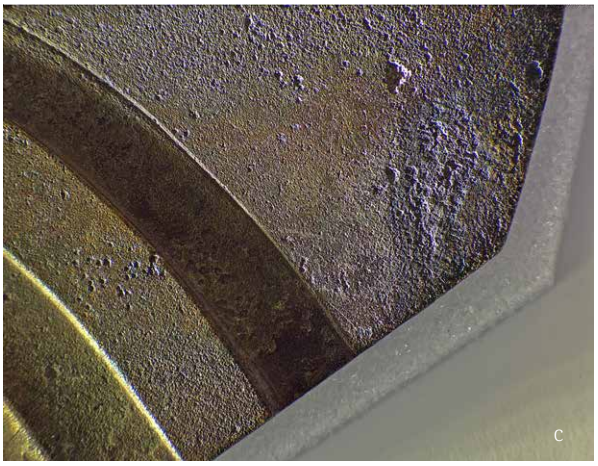

Figure 6.2: (a) X-ray; (b) MA-XRF Sn map; (c) VSC raking light of the handle of the dirk, grey area Sn corrosion products (RCE: Rijksdienst voor het Cultureel Erfgoed/Cultural Heritage Agency of the Netherlands).

excitation settings of 50 kilovolt with a corresponding current of 150 microampere, spotsize of 100 micrometres and a pixel scan time of 30 millisecond. Scanning was performed under ambient conditions. The M6 Jetstream uses a 30 square millimetres XFlash Silicon Drift Detector with an energy resolution < 145 eV for Mn Kα. PyMCA software was used to process the data.

Irradiation of the dirk in the neutron beam line causes the dirk to become temporarily radioactive. This radioactivity was measured with gamma spectroscopy (GS) to extract the tin concentration of the bulk of sword. Both the impinging neutron beam, as well as the subsequent emitted (and detected) gamma radiation penetrate the entire bulk of the dirk. Therefore, this combination of neutrons and gammas allows the determination of the elemental composition of the (pristine) bulk of the dirk. The tin concentration was extracted from the GS spectrum by analysis of the tin ^{125m1}Sn isotope and copper ^{66}Cu isotope.

6.3 Results and discussion

Using the non-invasive methods outlined above, the Ommerschans dirk was studied. A number of observations could be made that at least partially provide an answer to the questions posed.

6.3.1 Surface features

The surface of the dirk was first thoroughly examined using optical microscopy (Fig. 6.1). The surface is covered with pits. Corrosion processes may have enlarged them since porosity forms a starting point for corrosion. The patina appears uneven and composed of different corrosion products. These have not been analysed, but the green, red and black colours indicate the presence of copper carbonate, cuprous and cupric oxides. Typical signs of active corrosion were not observed.

Patches of silvery lustre and matt grey areas on the surface correspond to tin rich areas as seen in the XRF

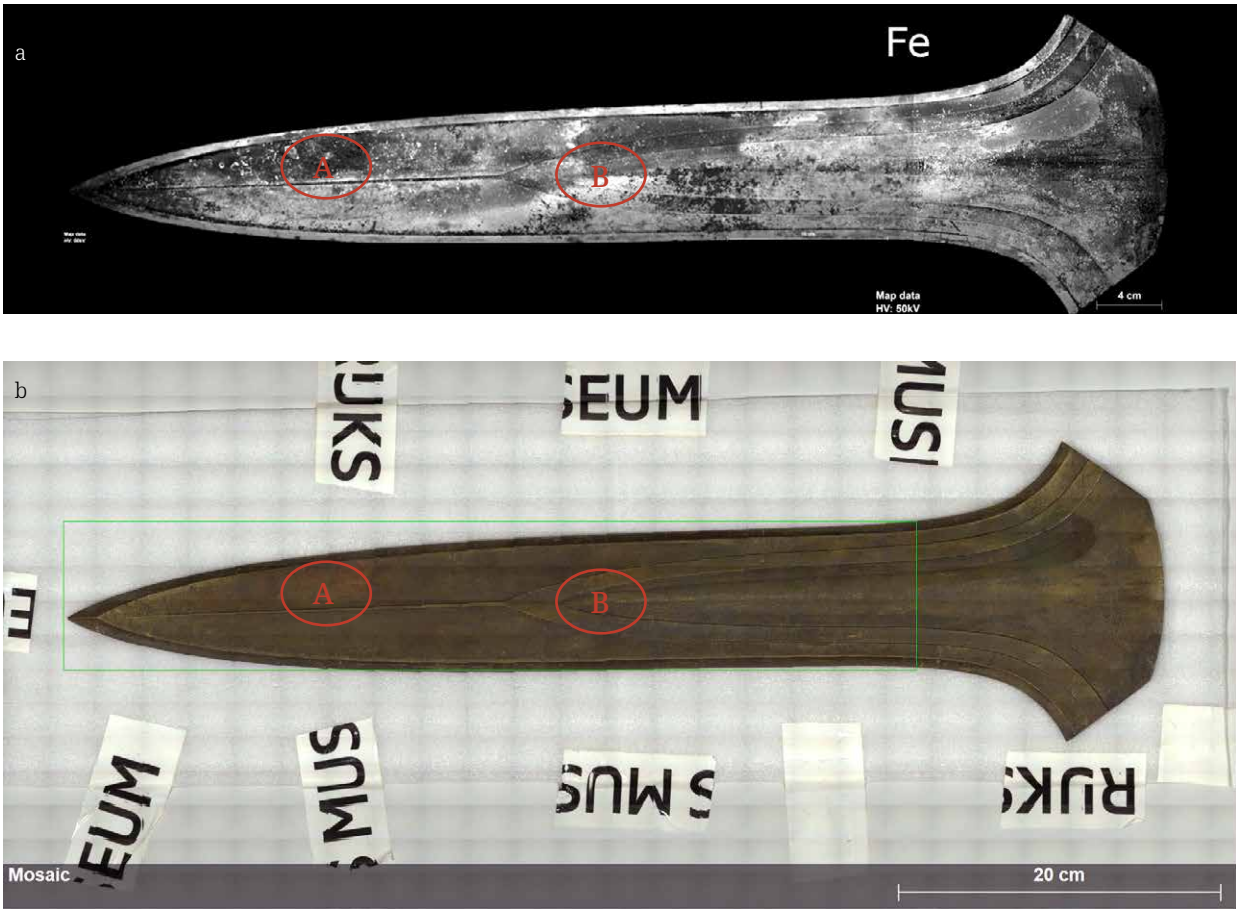

Figure 6.3: (a) MA XRF with Fe distribution, (b) video image and (c) a close up of area A made by the VSC (RCE).

mapping of tin (Fig. 6.2). These areas are not only visible on the broad part of the dirk but also along the edges (Fig. 6.9). All over the surface small spots with a high tin concentration are observed as well.

Like most prehistoric bronze artefacts, the Ommerschans dirk is made of low tin bronze (up to 17 wt% of Sn; Scott 2002, 401). It should be noted though that this implies the technical division between high and low tin bronze (high tin >17% being the maximum theoretical limit of the solubility of tin in the copper-rich solid solution, in practice this number is 14%), based on many different objects from different ages. In fact when compared to other bronze age artefacts from Europe, the Plougrescant-Ommerschans dirks in fact contain a high tin level (c. 14%) compared to most other bronze weapons and tools (see Arnoldussen *et al.* 2022, fig. 5)

In any case, high tin areas could be the result of the casting process or result from corrosion processes like decuprification. Tin sweat or inverse segregation is the result of the cooling down of the metal after casting (Van der Stok-Nienhuis 2017, 63). Corrosion processes in the soil can also result in an enrichment of tin on the surface, as a result of decuprification, the preferential dissolution of copper (Van der Stok-Nienhuis 2017, 64). With the non-invasive analysis methods we have used, it was not possible to identify which process occurred. A polished cross-section of the dirk could visualise the micro structure of the bronze, but is not an option. Tin-rich areas are seen on the butt-end and the thin edges of the dirk are also tin-rich (Fig. 6.2, b). Grey corrosion products are visible on the broadened butt end as well (Fig. 6.2, c). On the X-ray

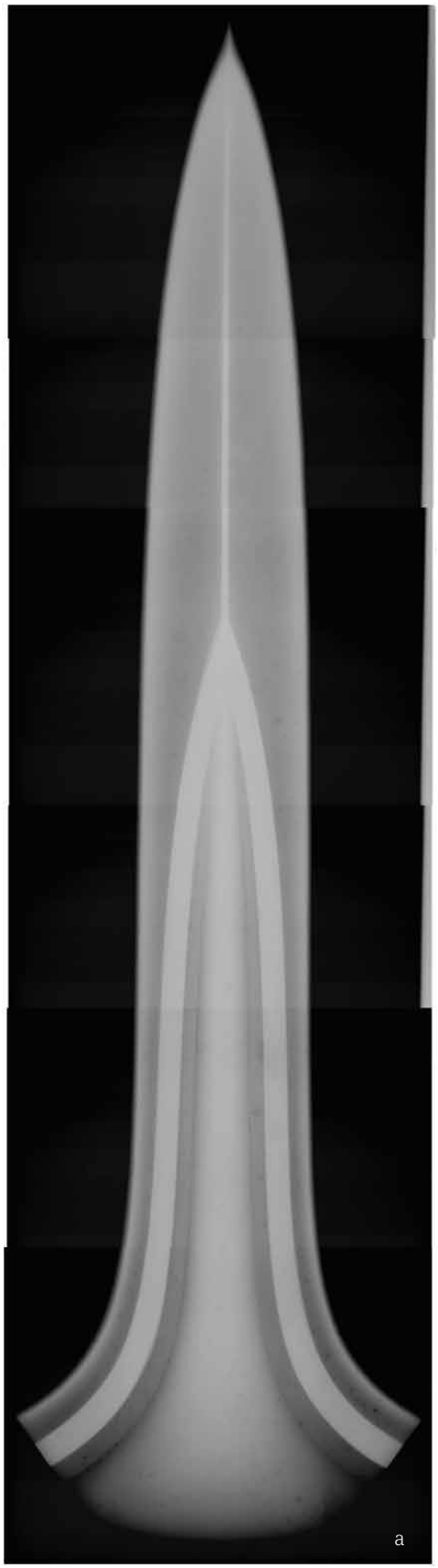

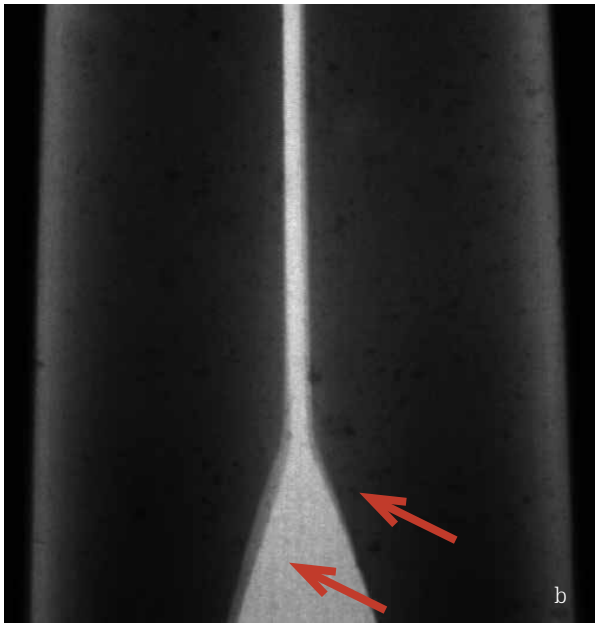

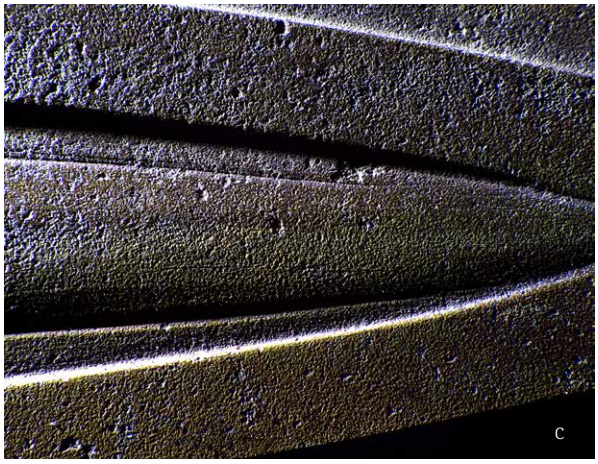

Figure 6.4: (a-b) X-ray images, 180 keV; (c) VSC image, raking light, the decoration on the sword is not symmetrical and worked afterwards (RCE).

Figure 6.5: (opposite page) Rendering of the 3D nCT computer model of the dirk. One clear artefact is the block-shaped feature somewhat to the right of the centre: this is caused by the computer-stitching of the 3rd and 4th nCT datasets and does not relate to the dirk. The second artefact on the right of the picture is the apparent transparency of the dirk on two symmetric locations of the hilt. This is a computer reconstruction artefact caused by low counting statistics when the neutron beam traverses the widest part of the dirk (19 centimetres, in this figure from top to bottom) (TU Delft Reactor Institute).

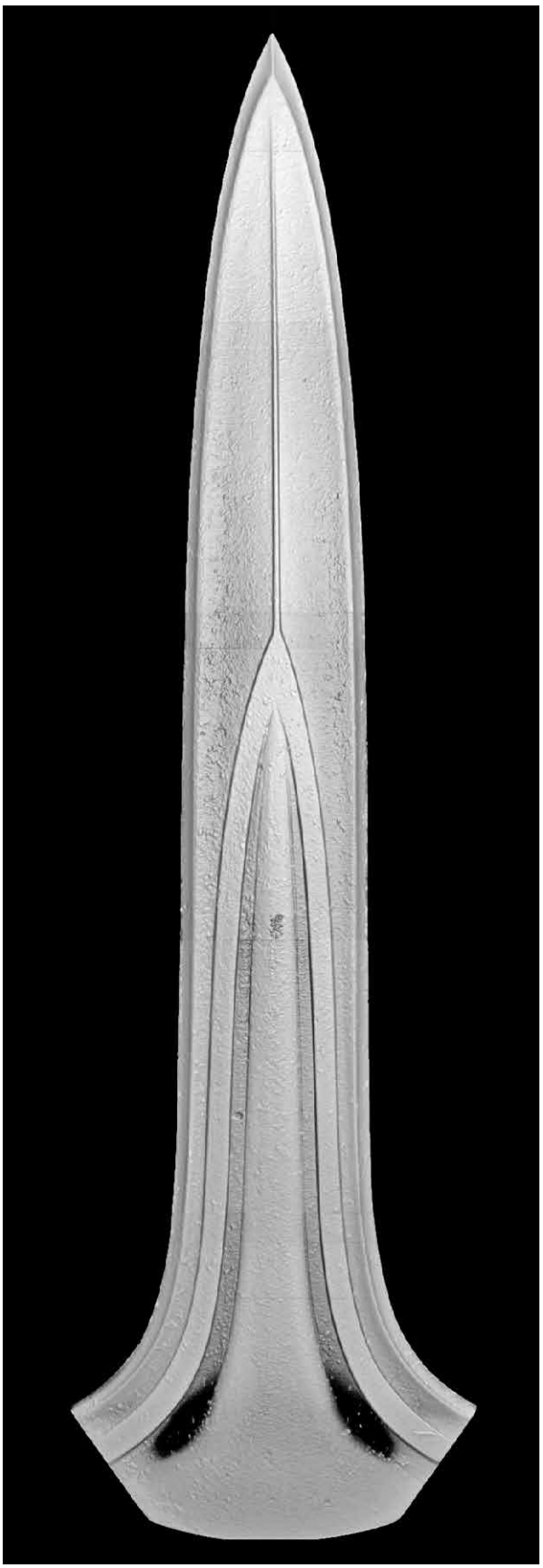

image a crack is visible (Fig. 6.2, a). This crack could be a shrinkage crack or could have been caused by finishing activities such as hammering. Tin rich bronze is known to be more brittle (Scott and Schwab 2019, 144), which could explain why the crack occurred specifically here.

The surface furthermore shows several brown coloured areas (Fig. 6.3, b and c). Several of these areas appear to contain less iron in the surface (Fig. 6.3, a). This could be the result of objects being placed on the surface of the dirk or it could also be the result of the heterogeneity of the bog. Leaves or larger parts of wood could have been close to the surface of the dirk creating a micro-climate. However, the Fe element map does not demonstrate an overlap with all the brown stains (Fig. 6.3, a and b: areas A and B). The areas where iron is depleted could potentially be connected to the places where the other objects in the hoard were placed on top of the sword (as argued in the original reports of the find Chapter 2). Iron has enriched on the edges of these areas. Possibly, iron from the soil could not reach the surface of the dirk in these areas. However, the iron depletion seems to be rather irregular and does not follow every possible outline of the other objects in the hoard. The iron enrichment on the surface maybe connected to the local soil conditions (Chapters 2 and 3).

Notches are observed at regular distances on the edge of the dirk (Fig. 6.1). The corrosion on the surface inside the notches is similar to that on the surface of the dirk. Therefore, it is assumed that the notches were intentionally marked before deposition with a sharp pointed object, perhaps a flint or bronze chisel.

6.3.2 Non-symmetrical decoration and post-casting work

The decorative pattern seen on the surface of the dirk is not perfectly symmetrical on both sides. This is clearly seen on the X-ray radiography image (Fig. 6.4). This could have several reasons. If a full model of the sword was used, with the decoration on both sides, perhaps the execution of this model was not done perfectly symmetrical. The asymmetry only became visible through modern see-through visualisation techniques such as x-radiography and in the nCT 3D model. The asymmetry could also be evidence of the use of a one-sided model or pattern that was used to make a mould of both sides of the sword. This half model would have been pressed into the soft loam twice and then the two mould halves were assembled to form the mould to cast the dirk.

Because the nCT model is a 3D model, it enables looking at both faces of the dirk individually (front side shown in Fig. 6.5). To verify the hypothesis about the use of a half-model, as described above, the two faces of the dirk's 3D model were overlaid as shown in Figure 6.6. By careful overlaying of the front side and rear-side of the dirk (shown in respectively light-grey and blue), one can

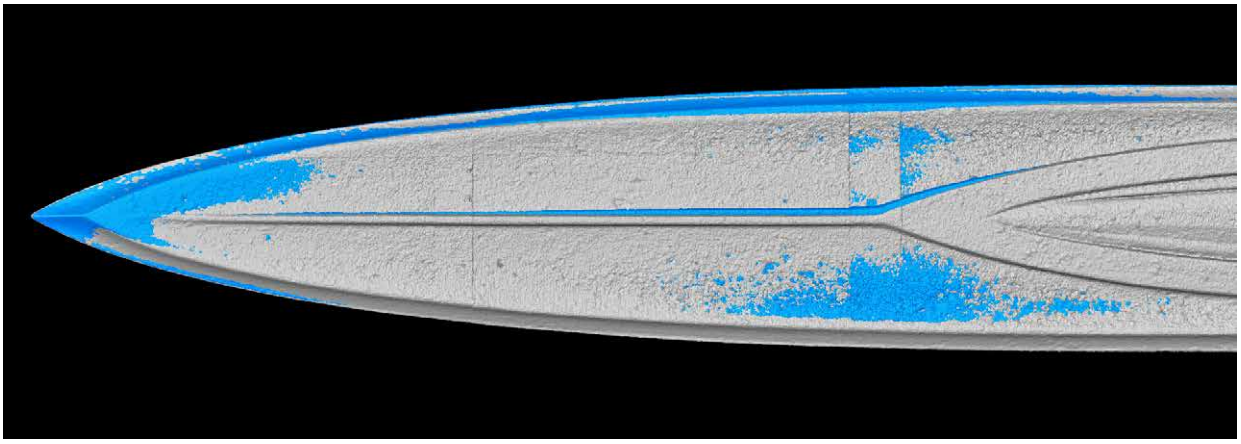

Figure 6.6: Two identical copies of the nCT 3D model of Figure 6.5 overlayed and aligned. The blue copy is rotated 180 degrees over the main axis of the dirk, so that this figure shows how the front side (grey) overlaps with the back side of the dirk (in blue) (TU Delft Reactor Institute).

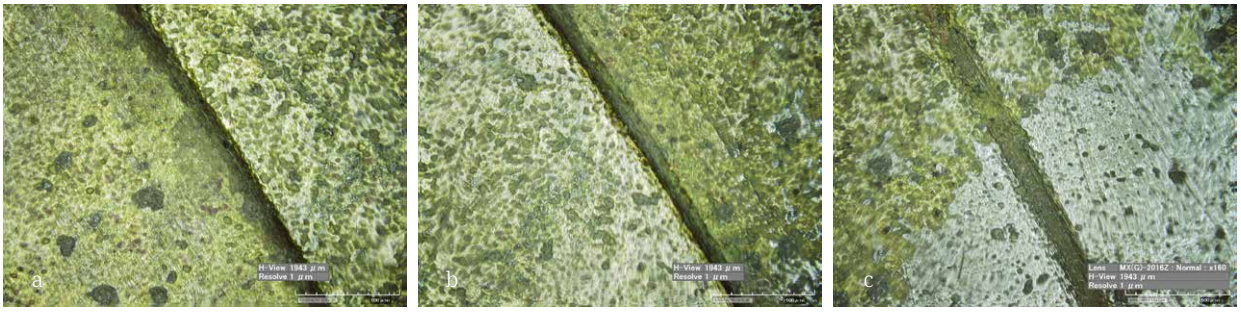

Figure 6.7: Section over the grooves on the dirk from outside to inside (a-c); see also Fig. 6.1 (TU Delft Reactor Institute).

clearly discern that the decorations on the two sides are not identical, meaning that the moulds of the respective sides are very similar, but unique. If one single mould would have been used for both faces, the light-grey and blue surfaces would overlap perfectly.

The cast decoration seems to have furthermore been worked with a tool (Fig. 6.7, a-c). The sharp lines on the sword suggest that the mould might have been made of a sturdy material like clay or stone (Fig. 6.7). The first line has a steep sharp edge, the other two seem to be grooves (Fig. 6.7, a-c). The depth of the grooves measures approximately between 0.5-1.5 millimetres.

The X-ray images show a high contrast for the metal (Fig. 6.8). The MA-XRF results show the material composition is heterogeneous, at least at the surface of the dirk (Fig. 6.9). The difference in contrast is most probably indicative for differences in thickness clearly showing the central rib and the decorative bands. The X-radiography shown in Figure 6.8 suggests porosity in the bulk of the hilt-side of the dirk. From the nCT 3D model one can see that these darker spots in the X-radiography are related to the surface of the two faces. In the nCT model, most of these spots appear as bright spot, which we tentatively relate to corrosion products, with higher chemical concentrations of hydrogen (nCT is particular sensitive to light elements). The lack of porosity in the dirk is seen in Figure 6.10. The same figure shows a rather clear porosity gradient visible in the nCT model of the replica dirk. This replica was industrially cast from the hilt.

The radioactivity that is generated by the neutron irradiation allows to determine the elemental composition of, specifically, the bulk of the dirk, through gamma spectroscopy. The tin concentration extracted from the GS experiments is shown in Figure 6.9, d shows it to be homogeneous along the dirk, within the accuracy of the measurements (also Table 6.1).

6.3.3 Traces of wear are visible on the dirk

The surface of the dirk may also have been re-polished after use, for instance to remove fingerprints, this could have been done with a polishing stone or even with fine-grained sand or clay. At the tip of the blade several polishing grooves are visible. Three larger grooves or nicks are visible on the higher outer rim, showing the

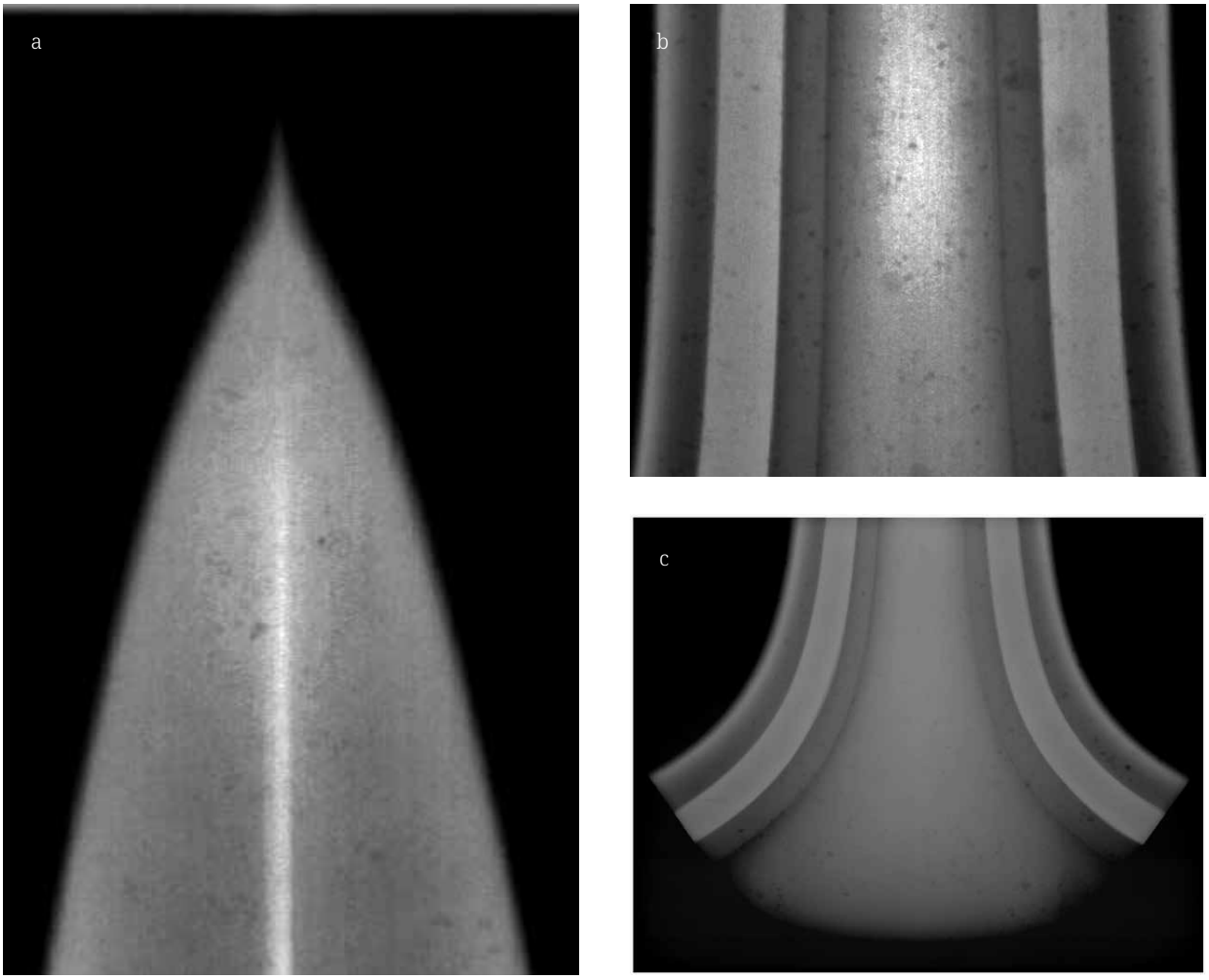

Figure 6.8: (a) Point; (b) Middle; (c) Hilt section. Grey scale variations indicate the presence of thicker and thinner parts visible as areas of high and low density (TU Delft Reactor Institute).

	Detected position	Cu	±	Sn	±	As	±	Sb	±	In	±	Ni	±	Pb	±
GS	Tip	83.2	1.2	16.8	1.2	0.38	0.07	0.134	0.011	0.00193	0.00007				
	Top	86.1	0.7	13.9	0.7	0.36	0.04	0.139	0.017	0.00181	0.00005				
	Mid	84.3	0.9	15.7	0.9	0.43	0.03	0.111	0.008	0.00182	0.00004				
	Bottom	85.3	0.8	14.7	0.8	0.40	0.04	0.113	0.006	0.00200	0.00005				
	Hilt	84.8	1.0	15.2	1.0	0.38	0.03	0.126	0.005	0.00170	0.00005				
XRF	XRF-dirk			14.5	0.5	0.335	0.025	0.095	0.015			0.52	0.05	0.14	0.01

Table 6.1: Composition in weight% of the dirk of Ommerschans from GS and XRF measurements.

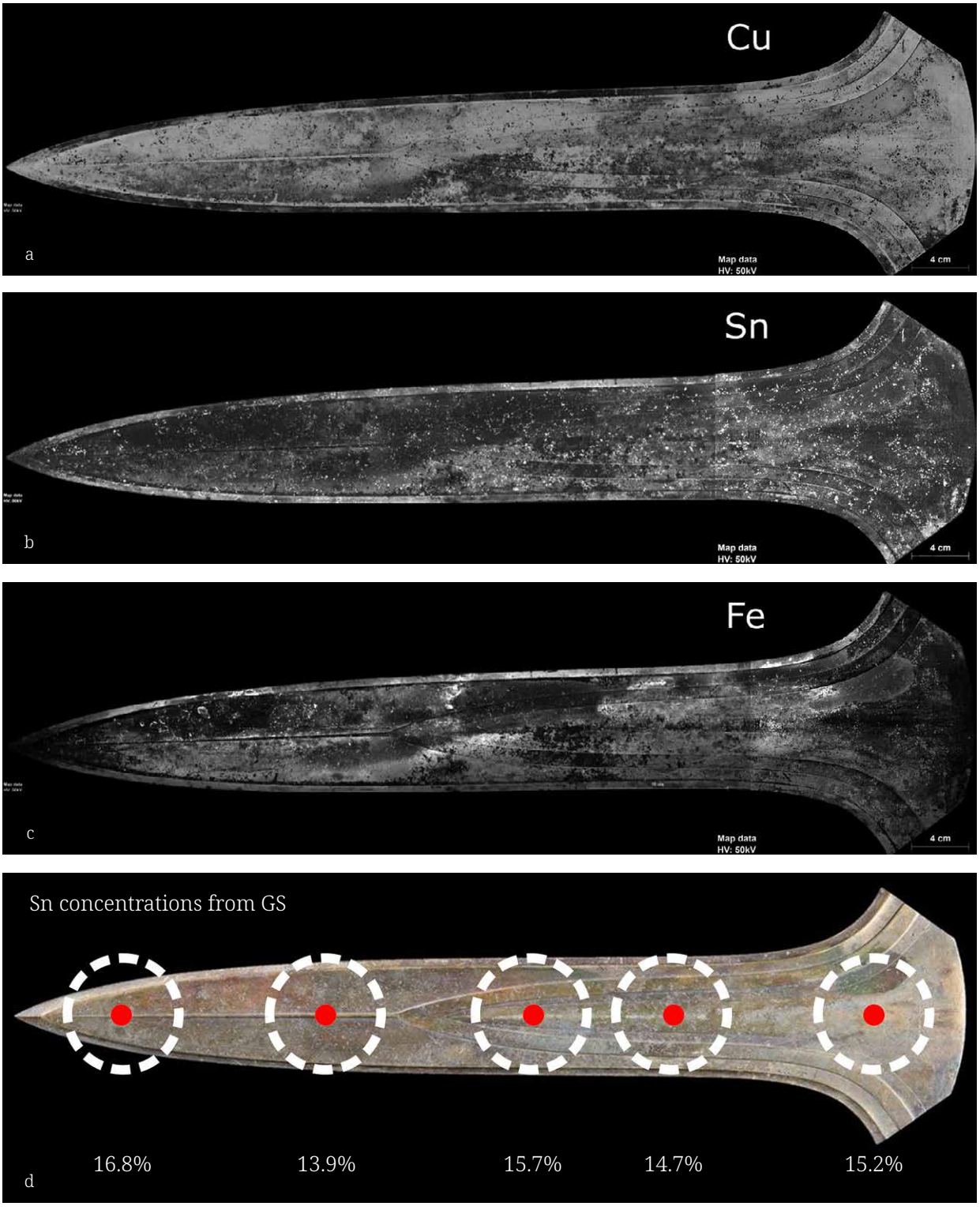

Figure 6.9: (a-c) MA-XRF element maps of Cu, Sn and Fe. Light areas are rich in the respective elements; (d) Distribution of Sn concentration along the length of the dirk. The marked measurement regions (dashed line) have the same size and shape as the collimator used. Although not many signs of polishing have been found on the surface, on the hilt side of side b of the sword a shiny polished part with fine grooves is visible (Fig. 6.11, b-c). The grooves also follow the decoration (Fig. 6.7, a). The sword most probably was polished to a shiny finish after casting (TU Delft Reactor Institute).

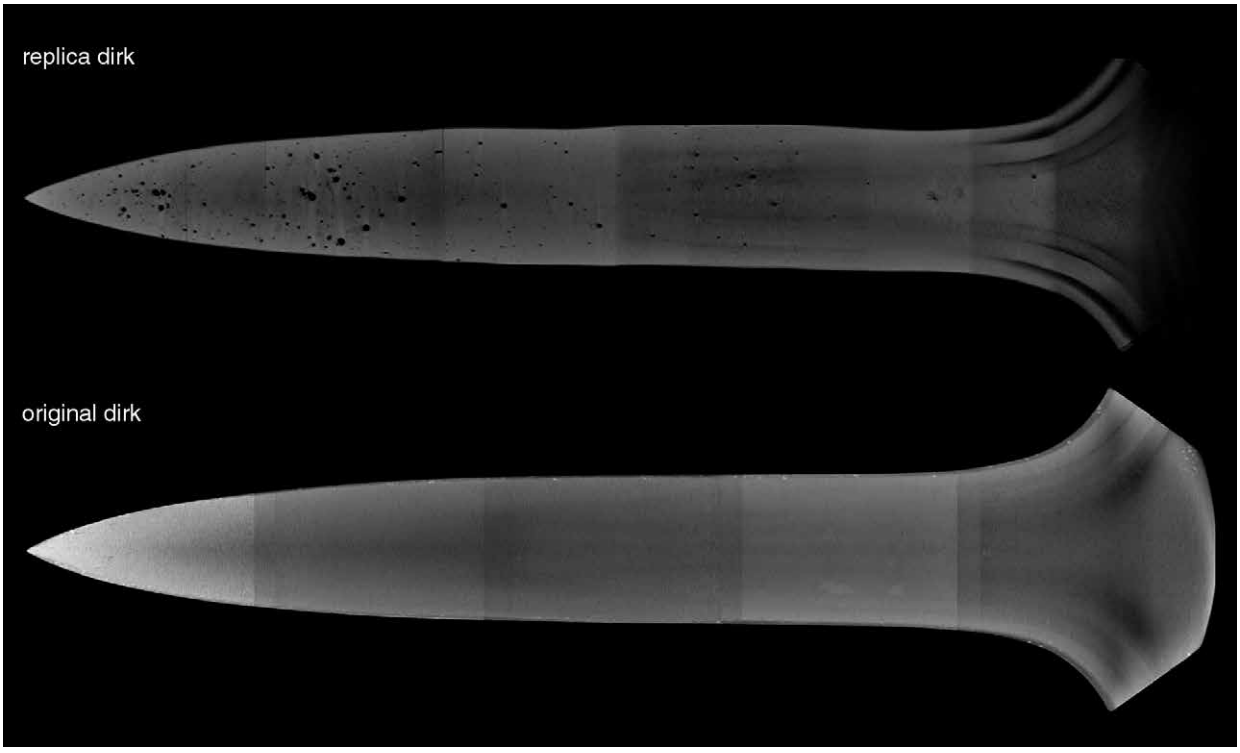

Figure 6.10: Slices through the bulk of nCT-scans of two dirks. The upper dirk is the replica made in Arnhem (RMO inv. no. *Z 2019/11.1*) which contains considerable porosity in the tip-section of the dirk, while the original Ommerschans dirk (bottom) is virtually free of porosity. Both images show computer artefact caused by the CT reconstruction, which explains the five 'vertical stripes' of different average grey values (TU Delft Reactor Institute).

Figure 6.11: VSC images. (a) Traces of wear and damage due to the excavation; (b-c) Polishing grooves on the point (RCE).

metal inside (Fig. 6.11, a). This is most probably a recent damage caused by a shovel when the dirk was found; the width of the grooves is very small (0.3-5 millimetres).

6.4 Conclusions

Combining the results of imaging the dirk with optical light, X-Radiography, neutron tomography and the chemical analysis by macro XRF and gamma spectroscopy, the following conclusions can be drawn:

The model was possibly made of wood and pressed in clay or loam. The two faces of the model are remarkably similar, but not identical, demonstrating the craftsmanship of its creator(s). The mould was used to cast the dirk in.

The internal homogeneity of the bulk of the dirk is remarkable, compared to the high porosity of the modern replica and the clear gradient in the porosity along the axis of the replica. The lack of porosity in the entire original bronze dirk is another demonstration of the craftsmanship of its creator(s).

The dirk was polished after casting probably to a shiny polished finish as indicated by striations and scratches. No traces of wear are visible on the surface.

References

Arnoldussen, S., Huisman, D.J., Van Os, B., Steffens, B., Theunissen, L. and Amkreutz, L. 2022. A not so isolated fringe: Dutch later prehistoric (c. 2200 BCE-AD 0) bronze alloy networks from compositional analyses on metals and corrosion layers. *Journal of Archaeological Science: Reports* 46, 103684 [doi.org/10.1016/j.jasrep.2022.103684]

Baron, J., Miazga, B. and Nowak, K. 2014. Functions and contexts of Bronze Age metal casting moulds from Poland. *Bulletin de la Société préhistorique française* 111/2, 325-338.

Beentjes, T.C.P. 2019. Casting Rodin's Thinker. *Sand mould casting, the case of the Laren Thinker and conservation treatment innovation*. Amsterdam: Unpublished PhD thesis.

Fontijn, D.R. 2001. Rethinking ceremonial dirks of the Plougrescant-Ommerschans type. Some thoughts on the structure of metalwork exchange, in: Metz, W.H., Van Beek, B.L. and Steegstra, H. (eds), *Patina. Essays presented to Jay Jordan Butler on the occasion of his 80th birthday*. Groningen/Amsterdam: Eigen beheer.

Garbacz-Klempka, A., Kwak, Z., Stolarczyk, T., Szucki, M., Żak, P.L., Ścibior, D. and Nowak, K. 2017. Reconstruction of the casting technology in the Bronze Age on the basis of investigations and visualisation of casting moulds. *Archives of Foundry Engineering* 17/3, 184-190.

Jennings, T.S. 1988. *Bellfounding*. Princes Risborough: Shire.

Kowalski, L., Garbacz-Klempka, A., Gackowski, J., Ścibior, D., Perek-Nowak, M., Adamczak, K. and Długosz, P. 2019. Towards direct casting: Archaeometallurgical insight into a bronze mould from Elgiszewo, Poland, 900-700 BC. *Archeologické rozhledy* LXXI, 45-66.

Kuijpers, M. 2008. Bronze Age metalworking in the Netherlands (c. 2000-800 BC). Leiden: Sidestone press.

Pola, A., Mödlinger, M. and Piccardo, P. 2015. Casting simulation of an Austrian Bronze Age sword Hilt. *Journal of the Minerals, Metals and Materials Society* 67, 1637-1645 [doi.org/10.1007/s11837-015-1464-y].

Sáez, C. and Lerma, I. 2015. Traceology on metal. Use-wear marks on copper-based tools and weapons, in: Marreiros, J., Gibaja Bao, J. and Ferreira Bicho, N. (eds), *Use-wear and residue analysis in archaeology*. Cham: Springer (= Manuals in Archaeological Method, Theory and Technique 1571-5752).

Scott, D.A. 2002. *Copper and bronze in art: corrosion, colorants, conservation*. Los Angeles: Getty Publications.

Scott, D.A. and Schwab, R. 2019. *Metallography in archaeology and art*. New York: Springer.

Van der Stok-Nienhuis, J. 2017. *Artefact biography 2.0. Acquiring more information from archaeological bronzes. An interdisciplinary study into corroded early iron age studs from Oss-Zevenbergen*. Delft: Unpublished PhD thesis Delft University.

Willer, F., Schwab, R. and Mirschenz, M. 2016/2017. Römische Bronzestatuen am Limes. Archäometrische Untersuchungen zur Herstellungstechnik. *Bonner Jahrbücher* 216, 57-120.

Zhou, Z., Plomp, J., Van Eijck, L., Vontobel, P., Harti, R.P., Lehmann, E. and Pappas, C. 2018. FISH: A thermal neutron imaging station at HOR Delft, *Journal of Archaeological Science: Reports* 20, 369-373 [doi.org/10.1016/j.jasrep.2018.05.015].